Silicon-based traveling-wave photodetector array (Si-TWPDA) with parallel optical feeding

Xianshu Luo*, Junfeng Song, Xiaoguang Tu, Qing Fang, Lianxi Jia, Ying Huang, Tsung-Yang Liow, Mingbin Yu, and Guo-Qiang Lo

*Institute of Microelectronics, A*STAR (Agency for Science, Technology and Research), 11 Science Park Road, Science Park II, Singapore 117685, Singapore*

**luox@ime.a-star.edu.sg*

Abstract: We demonstrate silicon-based traveling-wave photodetector arrays (Si-TWPDAs) with parallel optical feeding by integrating multiple Germanium photodetectors. Such Si-TWPDAs feature the merit of high optical saturation power with remaining the large operation bandwidth. The impedance-matched traveling-wave electrode design takes into account the individual Ge photodetector loading effect. Optical waveguide delay lines are designed in order to balance the electrical phase delay of the traveling-wave electrode. The maximum linear photocurrent at −4V biased voltage are respectively 16 mA, 38 mA, and 65 mA with integrating 1, 2, and 4 photodetectors, upon the saturation power of 40 mW, 100 mW, and 160 mW. This corresponds to a normalized photocurrent generation of >0.32 mA/μm^3 and a normalized saturation power of 0.8 mW/μm^3. The extracted fiber access responsivity is ~0.42 A/W and the intrinsic responsivity of ~0.82 A/W. The measured 3-dB bandwidth for 4-channel TWPDA is ~20 GHz.

OCIS codes: (040.6040) Silicon; (230.0230) Optical devices; (250.0250) Optoelectronics; (040.5160) Photodetectors.

References and links

1. J. Michel, J. Liu, and L. C. Kimerling, "High-performance Ge-on-Si photodetectors," Nat. Photonics **4**(8), 527–534 (2010).
2. D. A. B. Miller, "Device requirements for optical interconnects to silicon chips," Proc. IEEE **97**(7), 1166–1185 (2009).
3. J. Capmany and D. Novak, "Microwave photonics combines two worlds," Nat. Photonics **1**(6), 319–330 (2007).
4. C. H. Cox, *Analog Optical Links: Theory and Practice* (U.K. Cambridge Univ. Press, 2004).
5. C. H. Cox III, E. I. Ackerman, G. E. Betts, and J. L. Prince, "Limits on the performance of RF-over-fiber links and their impact on device design," IEEE Trans. Microw. Theory Tech. **54**(2), 906–920 (2006).
6. V. M. Hietala, G. A. Vawter, T. M. Brennan, and B. E. Hammons, "Travelling-wave photodetectors for high-power, large-bandwidth applications," IEEE Trans. Microw. Theory Tech. **43**(9), 2291–2298 (1995).
7. K. S. Giboney, M. J. W. Rodwell, and J. E. Bowers, "Traveling-wave photodetector theory," IEEE Trans. Microw. Theory Tech. **45**(8), 1310–1319 (1997).
8. S. Murthy, T. Jung, T. Chau, M. C. Wu, D. L. Sivco, and A. Y. Cho, "A novel monolithic distributed traveling-wave photodetector with parallel optical feed," IEEE Photon. Technol. Lett. **12**(6), 681–683 (2000).
9. M. Saif Islam, S. Murthy, T. Itoh, M. C. Wu, D. Novak, R. B. Waterhouse, D. L. Sivco, and A. Y. Cho, "Velocity-matched distributed photodetectors and balanced photodetectors with p-i-n photodiodes," IEEE Trans. Microw. Theory Tech. **49**(10), 1914–1920 (2001).
10. A. Beling, J. C. Campbell, H.-G. Bach, G. G. Mekonnen, and D. Schmidt, "Parallel-eed traveling wave photodetector for >100-GHz applications," J. Lightwave Technol. **26**(1), 16–20 (2008).
11. A. Ramaswamy, M. Piels, N. Nunoya, T. Yin, and J. E. Bowers, "High power silicon-germanium photodiodes for microwave photonic applications," IEEE Trans. Microw. Theory Tech. **58**(11), 3336–3343 (2010).
12. Z. Xiao, X. Luo, P. H. Lim, P. Prabhathan, S. T. H. Silalahi, T.-Y. Liow, J. Zhang, and F. Luan, "Ultra-compact low loss polarization insensitive silicon waveguide splitter," Opt. Express **21**(14), 16331–16336 (2013).
13. T. Y. Liow, K. W. Ang, Q. Fang, J. Song, Y. Xiong, M. Yu, G. Q. Lo, and D. L. Kwong, "Silicon modulators and germanium photodetectors on SOI: monolithic integration, compatibility, and performance optimization," IEEE J. Sel. Top. Quantum Electron. **16**(1), 307–315 (2010).
14. T.-Y. Liow, J. Song, X. Tu, A. E.-J. Lim, Q. Fang, N. Duan, M. Yu, and G.-Q. Lo, "Silicon optical interconnect device technologies for 40 Gb/s and beyond," IEEE J. Sel. Top. Quantum Electron. **19**(2), 8200312 (2013).

#213759 - $15.00 USD Received 9 Jun 2014; revised 15 Jul 2014; accepted 15 Jul 2014; published 12 Aug 2014

15. L. Y. Lin, M. C. Wu, T. Itoh, T. A. Vang, R. E. Muller, D. L. Sivco, and A. Y. Cho, "High-power high-speed photodetectors-design, analysis, and experimental demonstration," IEEE Trans. Microw. Theory Tech. **45**(8), 1320–1331 (1997).
16. A. E.-J. Lim, J. Song, Q. Fang, C. Li, X. Tu, N. Duan, K. K. Chen, R. P.-C. Tern, and T.-Y. Liow, "Review of silicon photonics foundry efforts," IEEE J. Sel. Top. Quantum Electron. **20**(4), 8300112 (2014).

1. Introduction

Ge-on-Si photodetector [1] is one of the key building blocks for the applications of silicon photonic based optical interconnect [2] and microwave photonics [3]. A photodetector with high power handling capability, namely high saturation photocurrent, and high operation speed is particularly important for analog optical link requiring high gain, low noise floor, and high spurious-free dynamic range [4, 5]. However, there is a trade-off between the photodetector operation bandwidth and the saturation power for the typical photodetector. In general, the conventional high-speed photodetector is designed with small absorption volume to ensure low capacitance and small carrier transit time, thus consequently cannot achieve high saturation power. In view of such tradeoff, various traveling-wave photodetector arrays in III/V material were proposed and demonstrated for high power and large bandwidth operation [6–10]. However, although silicon photonic has experienced unprecedented growth in the past decade, only limited effort has been devoted to address the high power handling issue using Ge-on-Si photodetector [11], with demonstration of up to 120 mA saturation photocurrent yet only 4.5 GHz of 3-dB bandwidth at −8V biased voltage due to the adoption of the large dimensional Ge structures (7.4 um width × 500 um length × 0.8 um thickness).

In this paper, we demonstrate, for the first time to the best of our knowledge, silicon-based parallel-fed traveling-wave photodetector arrays (TWPDAs) [3, 4] with multiple integrated Ge photodetectors, featuring the merits of large operation bandwidth as well as high optical power handling capability. We design the impedance-matched traveling-wave electrode considering the periodic loading effect originated from the individual Ge photodetector. Dual-layer metal structure is adopted in order for easy design and layouting for the impedance-matched traveling-wave electrode. Furthermore, optical delay lines are adopted in each optical channel in order to balance the electrical phase delay. We fabricate such TWPDAs using CMOS-compatible fabrication process on an 8 inch SOI wafer with integrating up to four photodetectors. The measured 3-dB bandwidth is 20 GHz at bias voltage of −4 V for a 4-channel TWPDA. The maximum linear photocurrents at −4V bias voltage for 1-, 2-, and 4-channel TWPDAs are respectively 16 mA, 38 mA, and 65 mA, with the saturation input optical powers of 40 mW, 100 mW, and 160 mW. This suggests the normalized photocurrent of >0.32 mA/μm^3 and the normalized saturation power of 0.8 mW/μm^3. The extracted fiber access responsivity is ~0.42 A/W, corresponding to an intrinsic responsivity of 0.82 A/W.

2. Device design and fabrication

Figure 1 shows the block diagram of the proposed parallel-fed *N*-TWPDA. The input light is first split into multiple parallel channels by using low-loss power splitter, such as Y-splitter, or multimode interferometer (MMI) splitter. The light in each of the channel is separately detected by individual high-speed photodetector. The photocurrent is then collected by using impedance-matched traveling-wave electrode in order to maintain the high-speed operation. Furthermore, the optical delay lines are introduced in each optical channel in order to balance the electrical phase delay induced by the traveling-wave electrode.

#213759 - $15.00 USD Received 9 Jun 2014; revised 15 Jul 2014; accepted 15 Jul 2014; published 12 Aug 2014

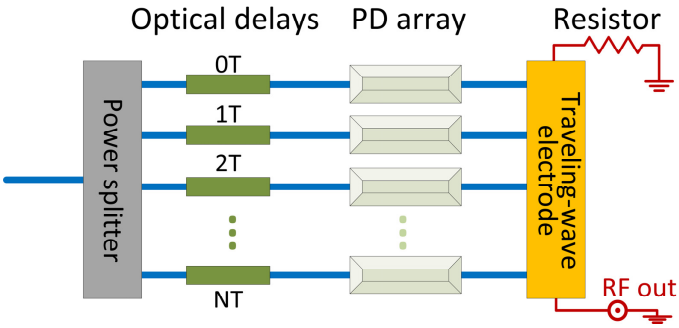

Fig. 1. The block diagram of an *N*-channel parallel-fed traveling-wave photodetector array, which includes power splitter, optical delay lines, Ge PD array and traveling-wave electrode.

Figure 2 shows the design layout of a 4-channel parallel-fed traveling-wave photodetector array (4-TWPDA). We adopt 2-stage 1 × 2 MMI splitter for the light splitting, which is modified from our previous design with extremely low loss [12]. The photodetectors adopted here is IME's baseline Ge photodetector with high operation speed [13, 14]. There are two different designs considering the orientations of the Ge photodetector and the traveling-wave electrode, namely parallel and orthogonally intersecting directions. For either case, the design of the traveling-wave electrode (metal width, gap width, etc.) is limited by the dimension of the Ge photodetector, which is normally 5μm × 20μm for high-speed operation. The dual-metal design releases the design restriction a lot for the traveling-wave electrode. Figures 2(b) and 2(c) show the zoom-in cross sectional views of such dual-metal design at positions of B and C in Fig. 2(a). The first metal layer connects to individual Ge photodetector, while the top metal layer is the impedance-matched traveling-wave electrode. We design the impedance-matched traveling-wave electrode with considering the periodic photodetector loading effect [15]. For a symmetric GSG traveling-wave electrode design with 6 μm signal metal width and 4 μm gap separations, the calculated electrical phase velocity is ~7.5 × 10^7m/s. The Ge photodetector is designed with 5μm × 20μm, and the periodicity (spacing between adjacent photodetectors) is 25μm. For all the traveling-wave electrode design, the ground metal widths are 100μm. Thus, based on the calculated electrical phase velocity, we design the waveguide-based optical delay lines with unit delay *T* of 0.3ps, which corresponds to the waveguide length of ~25 μm, assuming the group index of ~4 for the silicon waveguide.

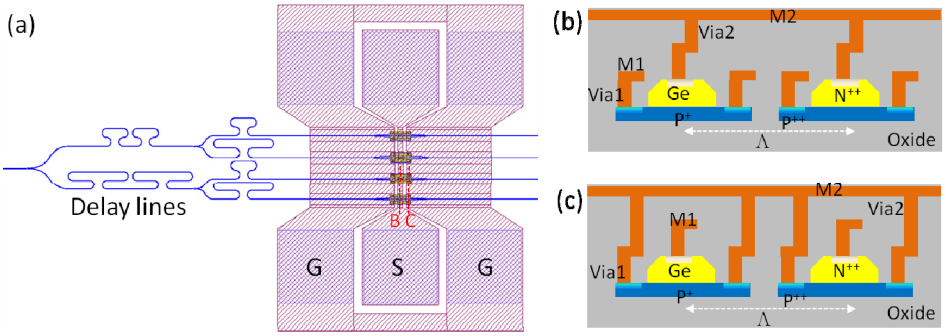

Fig. 2. (a) Design layout of a 4-channel TWPDA, including the 2-stage MMI-splitter for light splitting, the optical waveguide delay lines, and the Ge photodetector array integrating with the impedance-matched traveling-wave electrode with dual-meal layer. (b)-(c) The zoom-in cross-sectional views of the dual-metal layers design, corresponding to the positions B and C in (a).

We fabricate the TWPDAs in silicon-on-insulator (SOI) platform by using CMOS-compatible fabrication process [16]. The SOI wafer has a 220nm silicon layer sitting on a 2μm buried oxide (BOX) layer. The device is patterned by using deep ultra-violet (DUV)/248 photolithography, followed by a silicon reactive ion etching (RIE) to form channel

#213759 - $15.00 USD Received 9 Jun 2014; revised 15 Jul 2014; accepted 15 Jul 2014; published 12 Aug 2014

waveguides. For the Ge photodetector, separate masks are used for boron implantation to form the P region and P^+ contacts. The dopants are activated using rapid thermal anneal at 1050 °C for 5 seconds. After depositing a thin layer of field oxide, Ge epitaxial windows are opened by a combination of dry and wet etching to expose the underlying Si. After growing a thin SiGe buffer layer at 350 °C, Ge is selectively grown in an ultrahigh vacuum chemical vapor deposition (UHVCVD) epitaxy reactor at 550 °C with a thickness of 500 nm. The N^+ Ohmic contact is formed by implanting phosphorus into Ge top surface, followed by annealing at 500 °C. A 0.6 μm-thick oxide insulating layer is deposited, followed by the first contact holes opening, and the deposition and patterning of the first Al metal layer. After another 1.5 μm insulating oxide deposition, the second contact holes to the first metal layer are opened by dry etching process, followed by second Al metal deposition and patterning for the traveling-wave electrode.

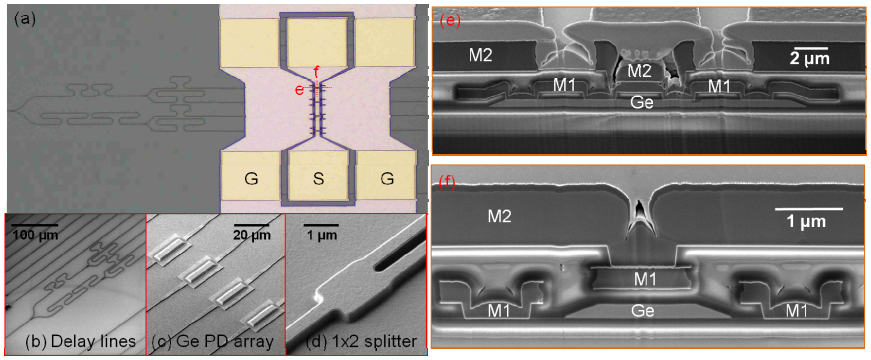

Fig. 3. (a) Optical microscope image of the fabricated 4-TWPDA. The SEM of (b) the optical delay lines, (c) the Ge photodetector array right after the Ge growth, and (d) the low-loss MMI splitter. (e) and (f) are the cross-SEMs (XSEMs) of the traveling-wave electrode with dual-metal layers.

Figure 3(a) shows the optical microscope image of the fabricated 4-TWPDA. We design and fabricate 1-, 2-, and 4-TWPDAs in the same silicon chip with identical designs. The waveguide width is 500 nm and the Ge photodetector is designed with dimension of 5μm in width and 20μm in length. The Ge photodetector periodicity is designed to be 25μm, with the optical delay line difference between adjacent channels of 25μm, in order for velocity matching between optical and electrical signals. Figures 3(b)-3(d) respectively show the SEMs of the waveguide delay lines, the Ge photodetector array right after the Ge growth, and the low-loss 1 × 2 MMI splitter. Figures 2(e)-2(f) show the cross-sectional views of the vertical structures in both directions, showing the dual-metal layer designs.

3. Device characterization

We first characterize the optical performance of the relevant building blocks, including the waveguide propagation loss, the MMI splitter insertion loss, etc., in order for the Ge PD responsivity extraction. By using the waveguide cutback structures, we obtained the waveguide propagation loss of −1.5 dB/cm, and the fiber-to-waveguide coupling loss of ~2.5 dB/facet. By using the multi-staged 1 × 2 MMI splitter structures, we obtained the splitter excess loss of −0.15dB/junction, which is consistent with our previous results [12].

#213759 - $15.00 USD Received 9 Jun 2014; revised 15 Jul 2014; accepted 15 Jul 2014; published 12 Aug 2014

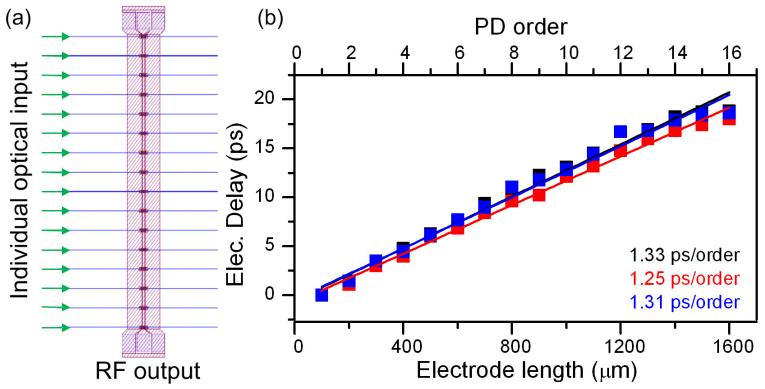

Fig. 4. Characterization of the phase velocity of the traveling-wave electrode. (a) Design layout of a 16 order traveling-wave photodetector array with individual optical input. (b) The measured electrical delay as function of the PD order for three randomly chosen devices with identical design in a wafer.

We investigate the phase velocity of the traveling-wave electrode by designing a multiple-channel parallel-input traveling-wave photodetector array, as shown in Fig. 4(a). The design of the photodetector and the traveling-wave electrode are the same as those of TWPDA, yet with increased Ge photodetector periodicity of 100μm for ease of delay characterization. By individually inputting optical signal from each of the input waveguide and detecting the electrical signal from the traveling-wave electrode, the electrical delay induced by the different length of the traveling-wave electrode is obtained. Figure 4(b) shows the measured electrical delay as function of the PD order, thus the electrode length, for three randomly chosen devices with identical designs in the same wafer. The extracted electrical delay is ~1.3 ps/order, suggesting a velocity of 7.7×10^7 m/s, which is very close to the calculation result of $\sim 7.5 \times 10^7$ m/s.

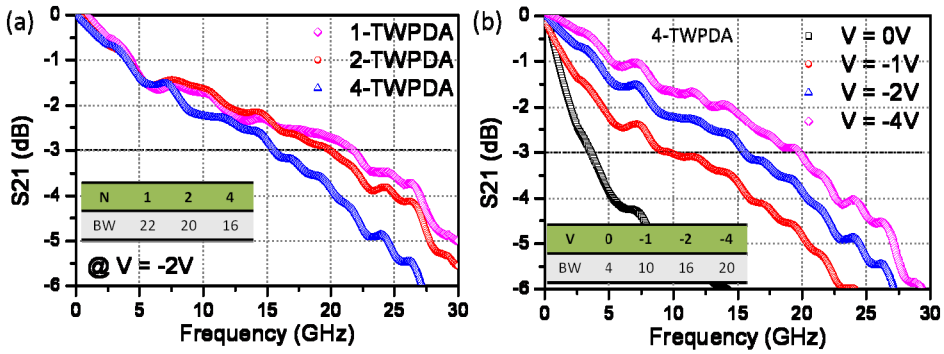

Fig. 5. Characterization of the operation bandwidth of the traveling-wave photodetector array. (a) S21 for 1-, 2-, and 4-TWPDAs at –2V bias voltage. (b) S21 for 4-TWPDA at 0V, –1V, –2V, and –4V baised voltages. The 3-dB bandwidth is summarized in the tables inserted.

We then measured the optical-electrical response of the fabricated TWPDAs by measuring the S21 parameter using a vector network analyzer (VNA). Figure 5(a) shows the normalized S21 for 1-, 2-, and 4-TWPDA upon –2V bias voltages. The measured 3-dB bandwidths are respectively 22 GHz, 20 GHz, and 16 GHz for 1-, 2-, and 4-TWPDA. The decrease of the 3-dB bandwidth with the increase of the Ge photodetector number suggests that further optimization of the traveling-wave electrode is still required in order to compensate the increased capacitance due to the parallel integration of the Ge photodetector array. Figure 5(b) shows the normalized S21 for 4-TWPDA upon different biased voltages. As the increase of the reverse biased voltages, the 3-dB bandwidth increases. The 3-dB

#213759 - $15.00 USD Received 9 Jun 2014; revised 15 Jul 2014; accepted 15 Jul 2014; published 12 Aug 2014

bandwidth at –4V biased voltage is ~20 GHz. For all the measurements, the corresponding 3-dB bandwidths are listed in the tables inserted.

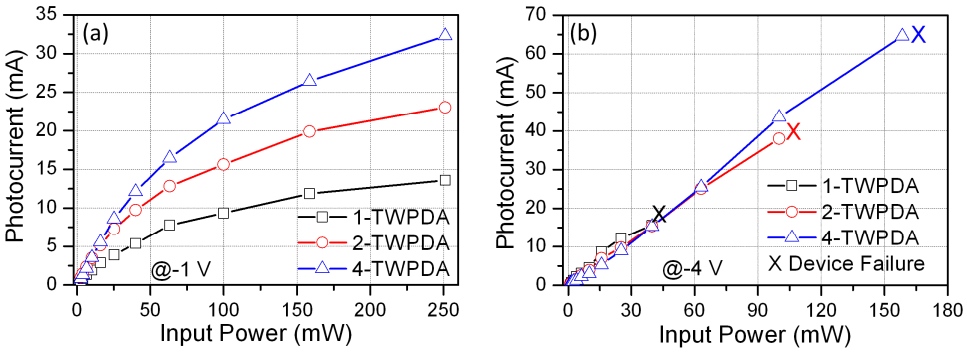

Fig. 6. Photocurrents characterization upon different optical input powers. The measured photocurrent of 1-, 2-, 4-TWPDA at (a) –1V and (b) –4V bias voltages. The maximum photocurrents before devices failure are respectively 16mA, 38mA, and 65 mA for 1-, 2-, and 4-TWPDAs.

We characterize the power handling capability by measuring the maximum linear DC photocurrent upon different optical input powers. In order to achieve sufficient optical power, we use a high-power Erbium-doped fiber amplifier (EDFA) to boost the input laser power which is only ~5mW. The power reaches to the DUT is controlled by a variable optical attenuator (VOA). The input power gradually increases from 1 mW to a maximum power of 250 mW (24dBm) and the corresponding photocurrents are measured. Figure 6(a) shows the measured photocurrent response for 1-, 2-, and 4-TWPDAs at –1V bias voltage. The input power is measured by directly connecting the input fiber to an external photodetector. The photocurrent quickly becomes saturated with less than 25 mW optical power, with maximum linear photocurrent of less than 10 mA for 4-TWPDA. The maximum photocurrents at 250 mW optical input are respectively 13mA, 23mA, and 32 mA. Figure 6(b) shows the photocurrent response with the input power increasing upon –4V biased voltage. The photocurrent linearity region significantly increases comparing to that with low biased voltages. The obtained maximum linear photocurrent are respectively 16mA, 38mA, and 65 mA for 1-, 2-, and 4-TWPDA, corresponding to the device failure powers of 40mW, 100mW, and 160 mW. This corresponds to a normalized photocurrent of 0.32 mA/μm^3, comparing to only 0.04 mA/μm^3 for the single Ge photodetector [11]. The fiber-access responsivity for the TWPDA can be extracted by linearly fitting the photocurrent-power curves, which is ~0.42 A/W. Considering the fiber-to-waveguide coupling loss of ~2.5 dB, and the MMI splitter loss of ~0.15dB/junction, the extracted intrinsic responsivity is ~0.82 A/W.

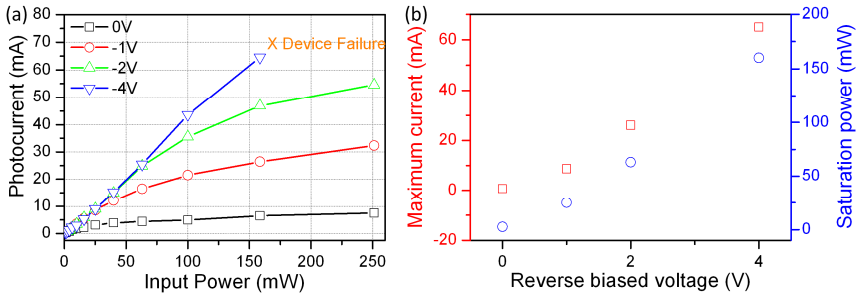

Fig. 7. (a) Photocurrent characterization of a 4-TWPDA upon different bias voltages with different optical input powers. (b) The extracted maximum photocurrent and the corresponding optical saturation powers.

#213759 - $15.00 USD Received 9 Jun 2014; revised 15 Jul 2014; accepted 15 Jul 2014; published 12 Aug 2014

Figure 7(a) shows the photocurrent response of a 4-TWPDA with different input optical power upon different biased voltages. As the increase of the reverse-biased voltage, the maximum linear photocurrent increases. Figure 7(b) shows the extracted maximum linear photocurrent as function of the reverse-biased voltage, together with the corresponding optical saturation powers. The saturation power increase from ~2.5 mW with 0V voltage to 160 mW at −4V biased voltage, with maximum photocurrent increase from 0.8 mA to 65 mA.

3. Summary

We have demonstrated silicon-based traveling-wave photodetector arrays (TWPDAs) with parallel optical feeding to Ge photodetector array. The impedance-matched traveling-wave electrode is designed with considering the individual Ge photodetector loading effect. Optical delay lines using low-loss waveguide are designed to balance the electrical phase delay. We demonstrated up to 4-channel TWPDA with 3-dB bandwidth of ~20 GHz and intrinsic responsivity of ~0.82 A/W at −4V biased voltage. The maximum photocurrent increases from 16 mA for 1-TWPDA to 65 mA for 4-TWPDA, corresponding to the optical saturation power of ~160 mW. This corresponds to a normalized photocurrent generation of >0.32 mA/μm^3 and a normalized saturation power of 0.8 mW/μm^3. The design is scalable and the saturation photocurrent and optical power can be further enhanced by integrating more photodetectors. Such traveling-wave photodetector array has wide applications such as optical communication, optical interconnection, and analog fiber-optic link.

Acknowledgment

This work was supported by the Science and Engineering Research Council of A*STAR (Agency for Science, Technology and Research), Singapore under SERC grant number: 102 174 0174, and 122 331 0076.

#213759 - $15.00 USD Received 9 Jun 2014; revised 15 Jul 2014; accepted 15 Jul 2014; published 12 Aug 2014